

RESEARCH ARTICLE



Real Time Glaucoma Prediction Using Y-UNet Classifier via Hardware Software Co-Design SMART System

OPEN ACCESS**Received:** 23.11.2021**Accepted:** 10.01.2022**Published:** 31.01.2022

Citation: Priya SS, Sathiaseelan JGR (2022) Real Time Glaucoma Prediction Using Y-UNet Classifier via Hardware Software Co-Design SMART System. Indian Journal of Science and Technology 15(3): 115-126. <https://doi.org/10.17485/IJST/v15i3.2174>

* **Corresponding author.**

priya.it09@gmail.com

Funding: None

Competing Interests: None

Copyright: © 2022 Priya & Sathiaseelan. This is an open access article distributed under the terms of the [Creative Commons Attribution License](#), which permits unrestricted use, distribution, and reproduction in any medium, provided the original author and source are credited.

Published By Indian Society for Education and Environment ([iSee](#))

ISSN

Print: 0974-6846

Electronic: 0974-5645

S Sathiya Priya^{1*}, J G R Sathiaseelan²

¹ Department of Computer Science, Bishop Heber College, Bharathidasan University, Trichy, Tamil Nadu

² Associate Professor and Head, Department of Computer Science, Bishop Heber College, Bharathidasan University, Trichy, Tamil Nadu

Abstract

Objectives: To present a real-time algorithm that combines Yolov5 and UNet-based CNN predictions to classify small-sized images, particularly medical images. **Methods:** The proposed model combines the various phases of preprocessing, object detection, segmentation and classification through Kalman filter, Yolov5, U-net based on CNN. The model is derived from the three different datasets to create a novel classification algorithm for medical data. The dataset contains images of 136 glaucoma patients and 187 healthy images. **Findings:** The proposed Y-UNet classifier framework is used to classify glaucoma images based on their IOP and CCT from real-time dataset collection. The proposed framework accuracy of 98.75% is achieved in the run time performance at 0.18 seconds per image. The accuracy is higher by 1.66% and runtime performance reduced by 0.03 seconds when compared with standard classification methods. Additionally, threshold optimizer has minimized the overall losses and provides the most accurate result. **Novelty:** The Y-UNet classifier model proposed here enables the real-time glaucoma prediction tasks to be carried out through the use of a hardware-based system known as the Sensitive Mirror Analyzer and Retina Tracker. To the best of our knowledge, for the first time, the proposed algorithm has been implemented to improve the accuracy and run time performance.

Keywords: UNet; Yolov5; YUNet classifier; Sensitive Mirror Analyzer and Retina Tracker (SMART) system; Glaucoma disease

1 Introduction

Nowadays, glaucoma⁽¹⁾ is one of the major eye diseases affecting human beings. According to the World Health Organization, around 58 million people will have glaucoma by 2020 with a 10% bilaterally blind rate⁽²⁾. Although blindness is the most common outcome of glaucoma, even mild visual field loss can have detrimental effects on quality of life. This is why it is important that patients are diagnosed early and treated for visual impairment⁽³⁾. Since there are a number of factors that can trigger

the development of glaucoma, such as age, elevated IOP, and measures of CDR (Cup to Disk Ratio), it is difficult to diagnose and monitor individuals at risk of this condition. This is why the use of a Sensitive Mirror Analyzer and Retina Tracker (SMART) system that can continuously measure IOP is recommended⁽⁴⁾. The methods discussed are not intended to diagnose glaucoma, but they can help identify individuals at high risk of developing the condition. Although the average eye pressure is 15 millimeters Hg, the range of normal eye pressure ranges from 10 to 21⁽⁵⁾.

In⁽⁶⁾ proposed QNN-MLAIC model is a conceptual framework that describes various steps in the acquisition, preprocessing, and classification of aerial images. Inception with RCNN is performed with the Residual Network-v2 model, which is used as an object detector. Then, QNN is used as a classifier to classify the aerial images. The main issue with this model is that it needs to perform selective search. In⁽⁷⁾ proposed Nesterov-accelerated Adaptive Moment Estimation (NADAM) optimizer was improved the detection rate of the gated recurrent unit (GRU) model by taking into account the various hyper parameters. This optimizer showed the various phases of the detection. Still a lot of factors that can be done to improve the search.

In⁽⁸⁾ suggested model predictive control is formulated to address the real time energy management of a battery. It is performed by implementing the black widow algorithm for the optimal allocation of charging stations and renewable energy sources. Still, it not achieved better precision and lower the cost imbalance. In⁽⁹⁾ projected algorithm for feature selection based on an adaptive sampling-based anomaly detection method. It is also used to identify the most effective features. The method is optimized through an oppositional swallow swarm optimization algorithm. Although, it commonly used for analyzing massive data.

In⁽¹⁰⁾ projected to automatically detect eight different ophthalmological diseases from fundus images using R-CNN based approach. The proposed method achieved its objective by extracting deep features from the images. Although the method was able to achieve an accuracy of 89.54%, the data it collected was not as accurate as expected. In⁽¹¹⁾ involved extracting the data from various sources, including ground-truth images and Mask-RCNN models. The resulting annotations were then generated and analyzed to extract the deep key points. It doesn't detect objects that are affected by motion blur.

In⁽¹²⁾ improved KNN algorithm for image identification. But we need to determine the value of k and the computation cost for each instance. In⁽¹³⁾ proposed algorithms to aid in the diagnosis of patients with visionary disorders. Hybrid algorithms for deep neural networks and decision tree-based classifiers are proposed to be used for performing diagnosis. This tool is commonly used for analyzing only massive data.

In⁽¹⁴⁾ planned a system which consists of different classifiers such as Naive Bayes, AdaBoost, XGBoost, and Random Forest Classifier. The significance of the saccadic angle along the horizontal and vertical axis is also shown. Slow real time prediction is very difficult to implement.

In this research the various methods analyzed were Naive Bayes, Random Forest, Adaboost, and XG Boost. Those methods dependence is not strong enough to support small-sized medical image features and predictions.

2 Material and methods

The method was evaluated in three publicly-available databases: DRIVE, CHASE_DB1, and one Trichy Government Hospital database. It is mainly used for validating and improving the reliability of databases. The dataset is focused on eye diseases such as glaucoma and healthy eyes. Evaluation of proposed algorithm is performed using a DRIVE database containing fundus images from 158 patients (118 healthy and 40 glaucoma image), CHASE_DB which contain 101 fundus images (70 glaucoma image and 31 healthy images), and Trichy government hospital which contain (200 glaucoma and 255 healthy images) via python with Jupiter notebook software. The main 70% of the dataset is utilized for training while, the last 30% is utilized for testing.

The architecture of SMART system shown in Figure 1. The Raspberry Pi⁽¹⁵⁾ is a device that works seamlessly with the PC. Its smart mirror acts as a reflective surface, which can collect data about a person's visual health.⁽¹⁶⁾ A fundus camera is used to evaluate the eye using a light beam. The beams of light are directed toward the retina and produce an inverted image. The camera's built-in light source eliminates the need for an optical filter.

The training part consists of an algorithm that we developed to estimate the IOP values⁽¹⁷⁾ of transmitted optical signals using a camera that's running a reflectance technology. The validation part consists of a method that compares the data collected by the algorithm to the data obtained by reference measurements.

2.1 Y-UNet Classifier Algorithm

The proposed model Yolo and U-Net combines the weighted cross-entropy loss and the dice coefficient loss into an object function for data imbalance reduction. For classification, the proposed network modifies with adding three pass-through layers that is dense layer, activation layer and flatten layer.

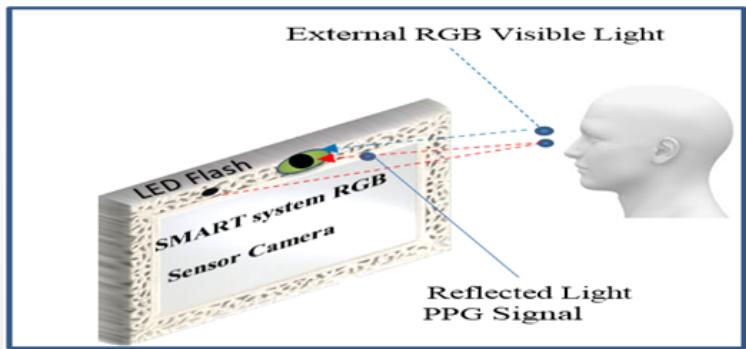


Fig 1. Architecture of SMART system

2.2 Pre-processing

Step 1: Create a function that uses probabilities and threshold to filter the boxes:

$$b_s = b_{cf} * b_{cp}$$

$$b_c = K \cdot \text{argmax}(b_s, -1)$$

$$b_{cs} = K \cdot \max(b_s, -1)$$

$$f_{mask} = b_{cs} > \text{threshold} (0.6)$$

$$S = b_{mask}(b_s, f_{mask})$$

$$B = b_{mask}(b_c, f_{mask})$$

$$C = b_{mask}(b_{cs}, f_{mask})$$

Here, box_confidence, box_scores, box_class_probs, box_classes, box_class_scores represents $b_{cf}, b_s, b_{cp}, b_c, b_{cs}$. And also, filtering_mask, scores, boxes and Classes indicates f_{mask}, S, B and C .

2.3 Object Detection

Step 2: Define a function to calculate the IoU between two boxes

$$b_{x1} = \max(\text{box1}[0], \text{box2}[0])$$

$$b_{y1} = \max(\text{box1}[1], \text{box2}[1])$$

$$b_{x2} = \min(\text{box1}[2], \text{box2}[2])$$

$$b_{y2} = \min(\text{box1}[3], \text{box2}[3])$$

$$\text{Area}_{\text{Overlap}} = (b_{x2} - b_{x1}) * (b_{y2} - b_{y1})$$

$$\text{Area}_{b1} = (\text{box1}[3] - \text{box1}[1]) * (\text{box1}[2] - \text{box1}[0])$$

$$\text{Area}_{b2} = (\text{box2}[3] - \text{box2}[1]) * (\text{box2}[2] - \text{box2}[0])$$

$$\text{Area}_{\text{union}} = (\text{Area}_{b1} + \text{Area}_{b2}) - \text{Area}_{\text{Overlap}}$$

$$\text{IOU} = \frac{\text{Area of Overlap}}{\text{Area of Union}}$$

Step 3: Define a function for Non-Max Suppression (NMS) is,
 $NMS = (B=B, S=S, \text{IoU_threshold}=0.6)$

Step 4: Select the box with highest objectiveness score

Step 5: compare the overlap of this box with other boxes

Step 6: Remove the bounding boxes with overlap >50%

Step 7: Move to the next highest objectiveness score

Step 8: Create a random volume of shape and then predict the bounding boxes.

Step 9: Define a function which will take the outputs of a CNN as input and return the suppressed boxes:

Step 10: Use the yolo_eval function to make predictions for a random volume:

$$S, B, C = \text{yolo_evaluation}(\text{yolo_output})$$

Step 11: Use a pre-trained YOLOv5 algorithm on new images

session = K.get_session()

Step 12: Define a function to predict the bounding boxes and save the images with these bounding boxes included.

Step 13: Read an image and make predictions using the predict function,

img_{shape} = float(img. shape [0]), float(img. shape[1])

S, B, C = yolo_evaluation (yolo_output , img_{shape})

Step 14: Plot the predictions

S_{out} , B_{out} , C_{out} = predict(sess, img)

Step 15: center of a bounding box (B_x, B_y), width (B_w), height (B_h) and value 'c' is resultant to a class of an object (such as, $humaneye_{right}$ and $humaneye_{left}$).

Y = (P_c, B_x, B_w, B_h)

Moreover, we have to predict the P_c value, which is the probability that there is an object in the bounding box.

2.4 Segmentation

Step 16: 3X3 convolutional : the general convolutional process, which is initiated by the 2d convolutional layers and this process increases the depth of the image.

$$b_{x,y,l} = ReLU \left(\sum_{i \in \{-1,0,1\}} \sum_{j \in \{-1,0,1\}} \sum_{k \in \{1, \dots, K\}} w_{i,j,k,l} (a_{x+i,y+j,k}) + c_l \right)$$

Step 17: 2X2 max-pooling: The max pooling process allows you to reduce an image's size by up to 572x572.

$$b_{x,y,k} = \max_{i,j \in \{0,1\}} a_{2x+i,2y+j,k} \rightarrow stride = 2$$

Step 18: 2x2 up-conv: this process expands the size of images.

$$b_{2x+i,2y+j,l} = ReLU \left(\sum_{k \in \{1, \dots, K\}} w_{i,j,k,l} a_{x,y,k} + c_l \right) \text{ for } i, j \in \{0, 1\}$$

$$= \sum_{\{x,y\} \in \Omega} w(x,y) \log_{pl(x,y)}(x,y)$$

$l : \Omega \rightarrow \{1, \dots, K\}$

Step 19: $(x,y) \rightarrow l(x,y)$ true label of each pixel

$$p_k(x,y) = \left(\frac{\exp(a_k(x,y))}{\sum_k^k \exp(a_k(x,y))} \right)$$

$$w(x,y) = w_c(x,y) + w_0 \exp \left(- \frac{(d_1(x,y) + d_2(x,y))^2}{2\sigma^2} \right)$$

$w_c(x,y) \rightarrow$ Weight map to balance class frequencies $w_{10} = 10$ & $\sigma \approx 5$ pixels

$d_1(x,y) \rightarrow$ Distance to the border of the nearest cell

$d_2(x,y) \rightarrow$ Distance to the border of the second nearest cell

Step 20: In the encoder, the image size gradually decreases as the depth increases.

$$Input (512x512x1) \Rightarrow Encoder \Rightarrow (8x8x1024) \Rightarrow Decoder \Rightarrow Output (512x512x1)$$

Step 21: In the decoder, the image's size increases and the depth decreases.

2.5 Classification

Step 22: Flatten the input image dimensions to 1Dimensional (width pixels x height pixels). Flattens an input of shape $n * c * h * w$ to a simple vector output of shape $n * (c * h * w)$.

Step 23: Normalization: The pixel values are normalized and the new minimum and maximum of 0.0 and 1.0

Step 24: One-Hot Encoder: converts a given categorical value into a new column and assigns a binary value to that column.

Step 25: With dense layers, build a model with structural design. The following attributes are used in the activation function of the program: activation function (x,y,z), weight matrix (xxx,x,y), and bias vector. The following attributes are used to represent a dense layer operation:

$$\text{Dense}_{\text{output}} = \text{activation}(\text{dot}(\text{input}, \text{kernel}) + \text{bias})$$

Step 26: Train the model and make predictions

A degenerative model is being developed to detect the degraded images. This model performed better in detecting degraded images and dealing with complex scenes. For shallow pedestrian features, the proposed network is modified to add three pass-through layers.

3 Dataset Implementation using our proposed model Y-UNet classifier

3.1 Object Detection

YOLO produces the corners of the rectangle, which are the coordinates of the U-Net output boxes. In this paper, we will show how to output the corners of a rectangular image using yolov5v. This method will enable us to crop the image properly. We have to find a threshold first to get the number of pixels that are not zero.

The distance formula is defined as:

$$D(\text{box}, \text{centroid}) = 1 - IOU(\text{box}, \text{centroid}) \tag{1}$$

Where D represents distance, box represents the sample, and centroid represents the center of the object, and $IOU(\text{box}, \text{centroid})$ represents the intersection of the object's center box and the object box. The final distance can be calculated as,

$$D(\text{box}, \text{centroid}) = \left[\frac{R_b \cup P_b - R_b \cap P_b}{R_b \cup P_b} \right] \tag{2}$$

Here, R_b represents the real box, and P_b represents the prediction box. As stated above, YOLOv5-nano algorithm has achieved end-to-end training and high-speed target detection shows in Figure 2.

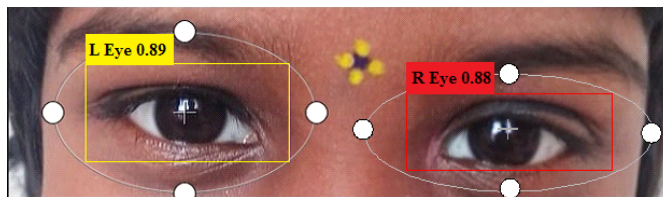


Fig 2. Boundary selection of Human eye

3.2 Feature Extraction of Pupil ratio

After extracting the desired image, the red layer is selected to reduce the data and make the picture look better. A morphological reconstruction technique is then used to remove the light reflections on the pupil. Adaptive thresholding⁽¹⁸⁾ is also applied to separate the background from the foreground in Figure 3.

The canny edge detection technique is used to detect the edges of the pupil and the iris. The circular Hough transform technique⁽¹⁹⁾ is then used to detect the radius and diameter of the pupil. For the calculation of the radius of a circle, R is known.

$$B_x = a + R\cos\theta \tag{3}$$

$$B_y = b + R\sin\theta \tag{4}$$

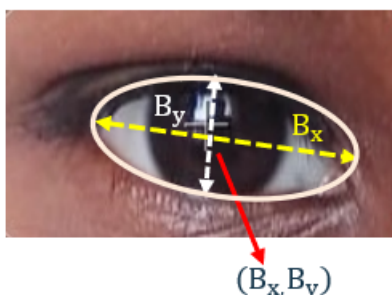


Fig 3. Pupil Ratio Extraction

3.3 Mean Redness Level of sclera area:

The mean red level is computed from the representation of the three values red, green, and blue. It is the representation of the red part of the pixel. To avoid the pixel being shifted to another color, the size of the red pixel should not exceed the size of the green or blue pixel values.

$$RL_{mean} = \frac{3x(m(R_{pixelvalue}) - m(G_{pixelvalue}) - m(B_{pixelvalue}))}{3x255} \tag{5}$$

where $m(R_{pixelvalue})$ relates to the mean of the red pixel values, $m(G_{pixelvalue})$ is the mean of the green pixel values, $m(B_{pixelvalue})$ is the mean of blue pixel values and RL_{mean} refers to the mean redness level.

3.4 Percentage of Red Area

The red area percentage RAP is the percentage of the red pixel in the extracted sclera. The computed Percentage of Red Area feature is the mean pixel percentage in the binary image that is represented by the RL_{mean} feature.

$$RA_{percentage} = \frac{\frac{1}{n} \sum_{i=0}^n R_{pixelvalue}(i)}{m} \tag{6}$$

Here, $R_{pixelvalue}(i)$ represents the red pixel values, 'n' indicates the total number of pixels in a region and 'm' refers to the total number of pixels in the extracted sclera.

In Figure 4, shows affected glaucoma eye image extraction, mean of redness level and redness area percentage computed by above formulae and Table 1 tabulated Ratio of pupil, mean redness level and pressure of redness area (Average for 323 Images)

Table 1. Ratio of pupil, mean redness level and pressure of redness area(Average for 323 Images)

	Pupil Ratio	Mean Redness Level	Redness Area Pressure
Normal	0.45	0.29	0.19
High Pressure	0.70	0.13	0.32

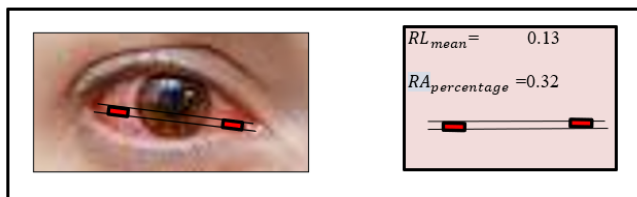


Fig 4. Sclera area Extraction, mean of Redness Level and Percentage of Red Area

3.5 Optic Disc and Cup Segmentation

This procedure is mainly used for disc smoothing. It uses ellipse fitting⁽²⁰⁾. It is also used for smooth cup boundaries. The video capture using a SMART system event camera. It shows the fundus image with a resolution of 320x320 pixels.⁽²¹⁾ A review of the various features selection techniques. The findings of the study and the comparative analysis of the available techniques were then summarized. In proposed method also used thresholding optimization method for segmentation, smoothing boundaries using ellipse fitting for optic disc segmentation and color thresholding⁽²²⁾ for optic cup segmentation in the segmentation part.

This procedure is mainly used for extracting blood vessels boundaries. It is also used for resizing, noise removal, and transformation. A patch classifier is composed of a disc and its receptive field is proportional to the size of the disc. Segmentation of optic cup and disc for evaluation process shows in Figure 5.

$$CIoU = IoU - \left(\frac{\text{center distance squared}}{\text{convex diagonal squared}} \right) - \left(\frac{v^2}{(1 - IoU) + v} \right) \tag{7}$$

$$LYUNet = 1 - CIoU \tag{8}$$

$$LUNet = 1 - IoU = 1 - \frac{\sum I_t o I_p}{\sum (I_t + I_p) - \sum (I_t o I_p)} \tag{9}$$

$$YUNet = L_{CIoU} + L_{UNet} \tag{10}$$

A fitting ellipse is executed to smooth the segmented framework⁽²³⁾. This method calculates an ellipse around all the pixels of a segmented outline.

The sum of the square off from the centroid to each pixel is then computed.

$$\text{Disc and Cup area distance} = \sqrt{(p - p_i)^2 + (q - q_j)^2} \tag{11}$$

The SMART technology helps in estimating the disc and ‘cup functional boundaries, which are also known as ONH. It also displays better information about the cup-to- disc ratio⁽²⁴⁾ and vertical and horizontal cup to disc area ratios. The ISNT rule can be easily analyzed in retinal fundus images by estimating the cup to disk ratio. The proposed method has given highest F1 score for disk and cup.

$$\text{Vertical cup - to - disc ratio } CDR_v = \frac{v_d}{v_c} \tag{12}$$

Here, v_d implies vertical disk; v_c implies vertical cup. Then will be compute vertical CDR.

$$\text{Horizontal cup - to - disc ratio} = CDR_h = \frac{h_d}{h_c} \tag{13}$$

Here, h_d implies horizontal disk; h_c implies horizontal cup. Then will be compute horizontal CDR.

Here compute accurate area of Central corneal thickness equation given below,

$$CCT(mm^2) = \left(\pi \frac{r}{4} \right) \times CDR_v(mm) \times CDR_h(mm) \tag{14}$$

Where CDR_v and CDR_h implies Vertical and Horizontal cup-to-disk ratio. CCT refers to Central corneal thickness.

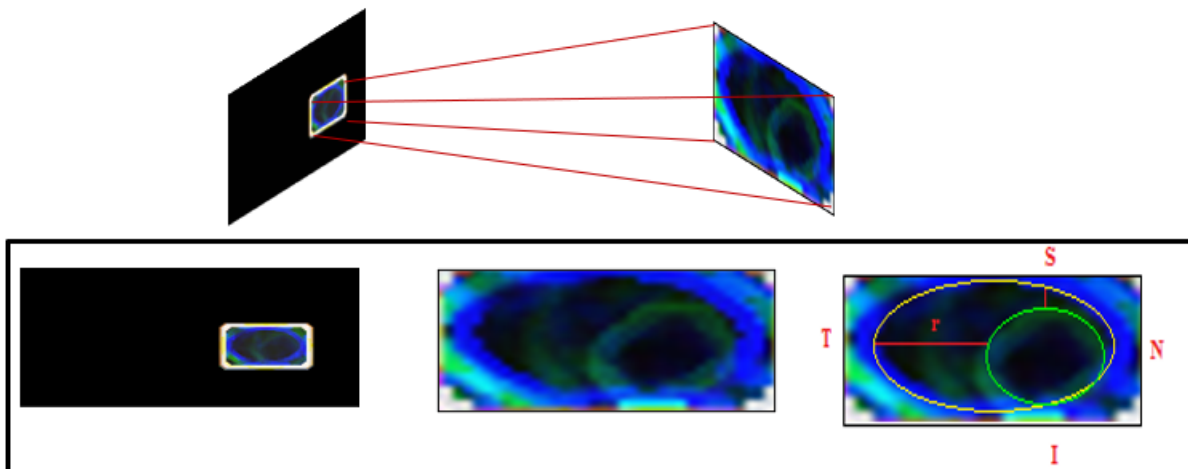


Fig 5. Segmentation of optic cup and disc for evaluation

3.6 Classification

The SMART system was built using the settings of the Y-UNet classifier. The status of the eye depended on the activation function of the network. The type of function that can be used to generate the activation values for the range between 0 and 1. It can also be related to the pupil/iris ratio. For example, if the pupil/iris ratio is greater than 1, then the higher value would be close to 1. Although the system does not count on a single feature, it uses a variety of features to make the final decision. The output range is used to differentiate between high and normal IOP. High IOP refers to the eye’s status as it relates to the pupil/iris ratio showed in Figure 6. The computed scaled value shows that the eye’s features did not create a high value. This means that it is likely to be classified as High IOP.

The Kalman filter⁽²⁵⁾ containing time derivative filters is used to decompose the ensemble average waveform. A set of features x describing the morphological appearance of a waveform is obtained and combined using a pre-training set of parameters. Derivative based morphological features of the Un-calibrated Intricate IOP.

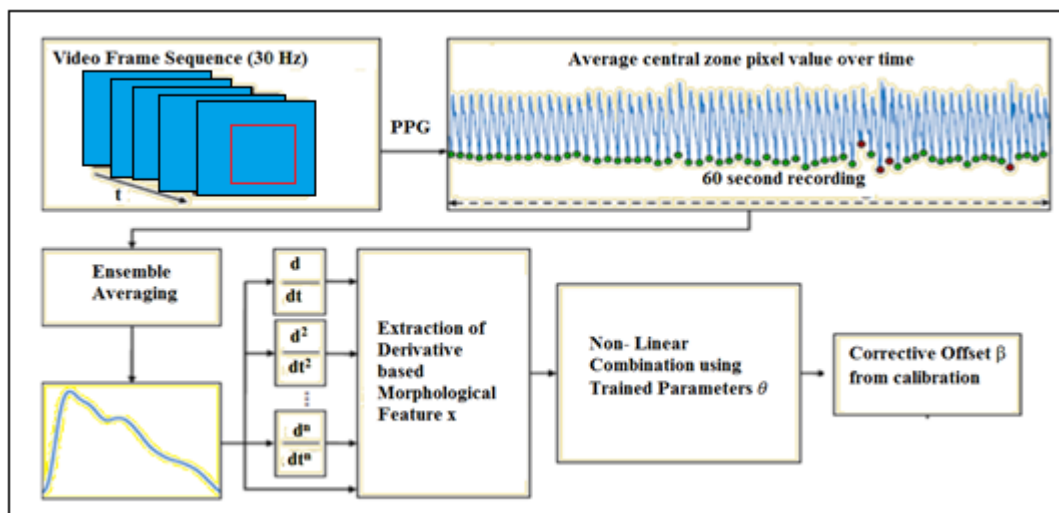


Fig 6. The process of the proposed algorithm

$$\text{IOP value Uncal}_{IOP} = f(\hat{\theta}, x) \tag{15}$$

Corrective offset $\hat{\beta}$ from calibration for final IOA derived OPP estimate

$$OPP_{IOP} = \text{Uncal}_{IOP} + \hat{\beta} \tag{16}$$

In this research have developed a SMART system that estimates blood pressure using three different measurement methods: reference systolic blood pressure, diastolic blood pressure, and mean blood pressure. The electronic patient record automatically calculated OPP values using the formula:

$$OPP_m = \frac{2}{3} * \left(\frac{2}{3} * DBP * \frac{1}{3} * SBP \right) - IOP \tag{17}$$

$$OPP_s = SBP - IOP \tag{18}$$

$$OPP_d = DBP - IOP \tag{19}$$

mOPP = mean ocular perfusion pressure, sOPP = systolic ocular perfusion pressure, dOPP = diastolic ocular perfusion pressure, DBP = diastolic blood pressure, SBP = systolic blood pressure and IOP = intraocular pres-sure.

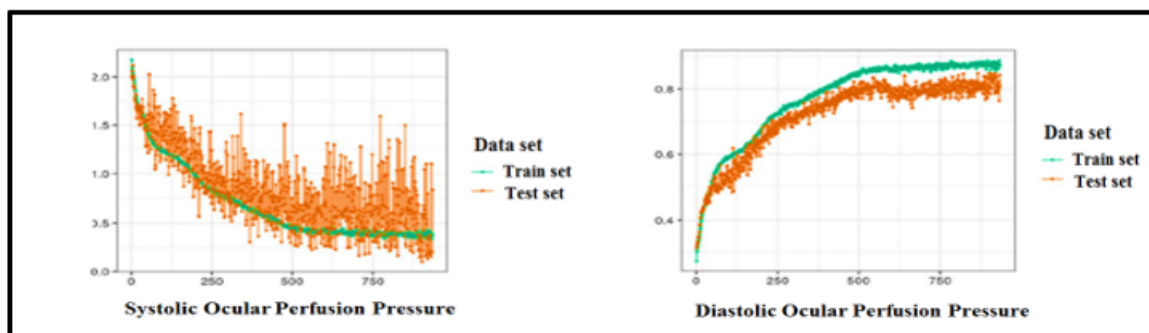


Fig 7. Training and Testing Performance of Systolic and Diastolic Ocular Perfusion Pressure

A training component and a validation component were proposed to implement this Model shows in Figure 7. The latter serves as the validation component for the system. This part aims to develop an algorithm that will estimate the IOP values from the transmission of Photo Plethysmo Grams (PPG) signals. The validation part of our system is designed to evaluate the accuracy of our algorithm when used by patients⁽²⁶⁾.

4 Results and Discussion

Our proposed method was evaluated against the results of standard glaucoma screening methods. The plot below shows the performance of the selected classifier. In this paper, we proposed a novel framework that uses non-invasive and automated methods to detect high-risk IOP and CCT using frontal eye images. Image processing techniques were then used to identify high-risk cases of eye pressure. This study analyzed 187 cases where the eye pressure was normal or high. The proposed model was developed in Python with Jupyter notebook. It was tested with a Y-UNet classifier.

The proposed framework investigated the relationship between the features extracted from an image and the intricate features of the eye (IOP and CCT). This study builds on the findings of our earlier studies, which indicated that early detection of IOP risk and CCT ratio could improve treatment decisions and reduce hospital stays. The Y-UNet framework is used to classify images. The framework achieves an accuracy of 98.75%.

Table 2. Run time performance and Accuracy for various classification algorithm

Algorithm	Navie Bayes	Ada Boost	Random Forest	XG Boost	The proposed Y-UNet Classifier
Run time (sec/img)	0.86	0.73	0.25	0.21	0.18
Accuracy %	66.25	83.2	83.2	97.09	98.75

Table 3. Healthy, Glaucoma suspects and Glaucoma subject Cases from real-time dataset (Average for 323 Images)

Category	Age	Sex			All Subjects (n=323)*		result of CCT		result of IOP		Healthy Subject (n=187)	Glaucoma Suspects (n=136)	Glaucoma Subjects (n=83)
		Male	Female	Total	Mean	SD	Mean	SD	Mean	SD			
1	below 6	13	15	28	14	1.41	0.13	0.12	18.5	7.9	14.97	18.18	3.37
2	7 to 17	33	25	58	29	5.66	0.14	0.12	19.2	9.4	31.02	37.66	6.99
3	18 to 40	36	27	63	31.5	6.36	0.17	0.11	20.3	9.8	33.69	40.91	7.59
4	41 to 75	42	36	78	39	4.24	0.18	0.14	22.6	7.3	41.71	50.65	9.4
5	above 76	47	49	96	48	1.41	0.16	0.02	24.0	8.6	51.34	62.34	11.57
Total	No. of study Population	171	152	323	32.3	3.82	0.16	0.10	20.9	8.6	34.55	41.95	7.78

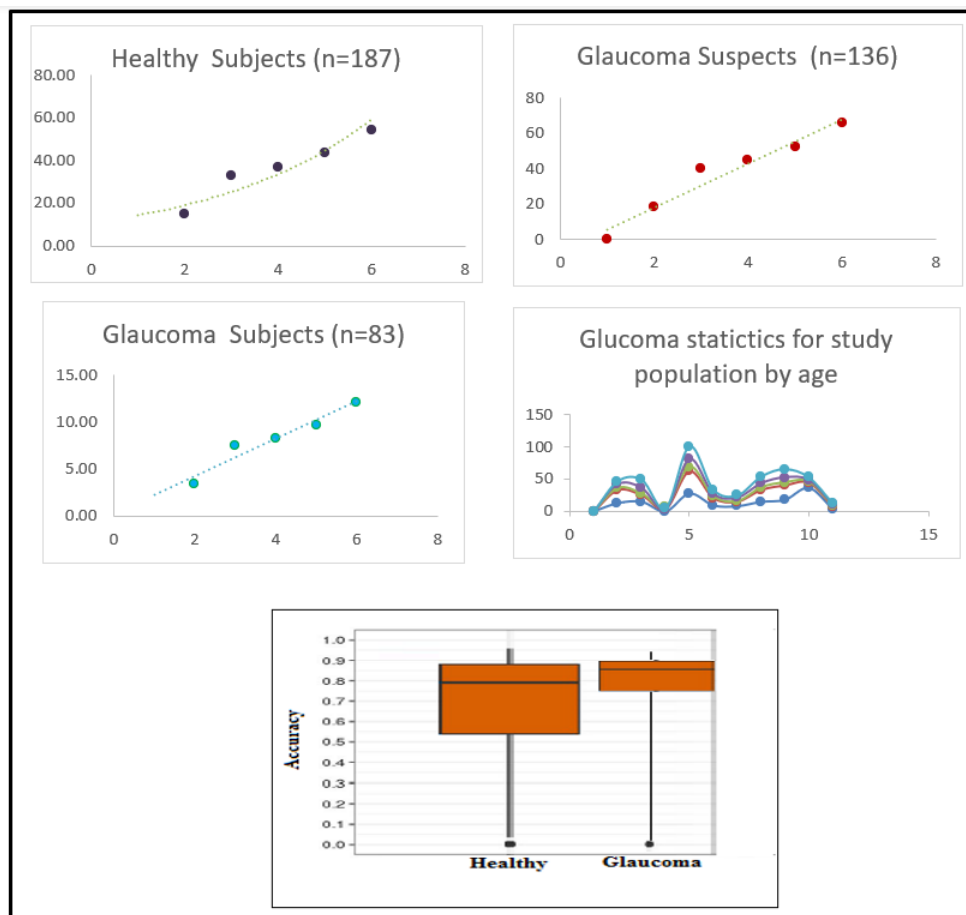


Fig 8. Graphical representation of Healthy, Glaucoma suspects and Glaucoma subject

A classification model tries to draw some conclusion from the input values given for training. It will predict the class labels or categories for the new data. The addition of a visual representation of the results of a CNN-based system is essential for its adoption in real clinical applications. The Table 2 shows the limitations of different classification algorithms. In our proposed model, Run time performance and Accuracy for various classification algorithm are tabulated.

Non-glaucomatous causes such as age, diabetes, and cataracts can be easily identified with the use of photos of the optic discs. A history of other conditions can also be helpful in the valuation of patients with suspected tension glaucoma. Table 3 shows the healthy and glaucoma suspect cases that were analyzed in real-time data, and their graphical representation is shown in Figure 8.

5 Conclusion

This study proposed Y-UNet classifier as a hybrid approach based on the yolov5 model, the UNet, and CNN. A unified proposed model to enable image classification with ease. It is built on top of existing frameworks and can be trained straight on full images. Various algorithms such as Adaboost, Naive Bayes, and Random Forest classifiers have improved their speed and accuracy. However, their slow classification has been a major bottleneck in real-time detection of images. This model performed better in detecting degraded images and dealing with complex scenes. In the experiments, this method has an accuracy of 1.66% and a runtime performance of 0.03 seconds lower than standard classification methods.

In the future, the SMART System can be implemented in hospitals for ease of eye diagnosis. It may also be developed for reading the full human body. It can also be developed as a simple and user-friendly equipment in our day-to-day life for monitoring our health conditions. By developing this system each and every part of the human body can be analyzed which will indicate every minor disorder. This can be developed for early detection of any disorder in any part of the human body.

Acknowledgements

The authors thank Dr. Parthiban Purushothaman, Ophthalmologist, Head of the Department, Ophthalmology, Government Hospital, Trichy, Tamilnadu, India, for providing required data set for this research work.

References

- 1) Nouri-Mahdavi K, Mohammadzadeh V, Rabiolo A, Edalati K, Caprioli J, Yousefi S. Prediction of Visual Field Progression from OCT Structural Measures in Moderate to Advanced Glaucoma. *American Journal of Ophthalmology*. 2021;226:172–181. Available from: <https://dx.doi.org/10.1016/j.ajo.2021.01.023>.
- 2) Allison K, Patel D, Alabi O. Epidemiology of Glaucoma: The Past, Present, and Predictions for the Future. *Cureus*. 2020;12(11). Available from: <https://dx.doi.org/10.7759/cureus.11686>.
- 3) Ganesh SS, Kannayeram G, Karthick A, Muhibbullah M. A Novel Context Aware Joint Segmentation and Classification Framework for Glaucoma Detection. *Computational and Mathematical Methods in Medicine*. 2021;2021:1–19. Available from: <https://dx.doi.org/10.1155/2021/2921737>.
- 4) Priya SS, Sathiaseelan JGR. Enhanced Retina Blood Vessel Segmentation by Super Resolution Generative Adversarial Networks based U-Net. *Indian Journal of Science and Technology*. 2021;14(43):3246–3253. Available from: <https://dx.doi.org/10.17485/ijst/v14i43.1502>.
- 5) Badakere SV, Chary R, Choudhari NS, Rao HL, Garudadri C, Senthil S. Agreement of Intraocular Pressure Measurement of Icare ic200 with Goldmann Applanation Tonometer in Adult Eyes with Normal Cornea. *Ophthalmology Glaucoma*. 2021;4(3):238–243. Available from: <https://dx.doi.org/10.1016/j.ogla.2021.04.002>.
- 6) Abdel-Khalek S, Algarni M, Mansour RF, Gupta D, Ilayaraja M. Quantum neural network-based multilabel image classification in high-resolution unmanned aerial vehicle imagery. *Soft Computing*. 2021. Available from: <https://dx.doi.org/10.1007/s00500-021-06460-3>.
- 7) Althobaiti MM, Kumar KPM, Gupta D, Kumar S, Mansour RF. An intelligent cognitive computing based intrusion detection for industrial cyber-physical systems. *Measurement*. 2021;186:110145–110145. Available from: <https://dx.doi.org/10.1016/j.measurement.2021.110145>.
- 8) Aljehane NO, Mansour RF. Optimal allocation of renewable energy source and charging station for PHEVs. *Sustainable Energy Technologies and Assessments*. 2022;49:101669–101669. Available from: <https://dx.doi.org/10.1016/j.seta.2021.101669>.
- 9) Mansour RF, Abdel-Khalek S, Hilali-Jaghdam I, Nebhen J, Cho W, Joshi GP. An intelligent outlier detection with machine learning empowered big data analytics for mobile edge computing. *Cluster Computing*. 2021. Available from: <https://dx.doi.org/10.1007/s10586-021-03472-4>.
- 10) Demir F, Taşçı B. An Effective and Robust Approach Based on R-CNN+LSTM Model and NCAR Feature Selection for Ophthalmological Disease Detection from Fundus Images. *Journal of Personalized Medicine*. 2021;11(12):1276–1276. Available from: <https://doi.org/10.3390/jpm11121276>.
- 11) Nazir T, Irtaza A, Starovoirov V. Optic Disc and Optic Cup Segmentation for Glaucoma Detection from Blur Retinal Images Using Improved Mask-RCNN. *International Journal of Optics*. 2021;2021:1–12. Available from: <https://dx.doi.org/10.1155/2021/6641980>.
- 12) Fan Z, kun Xie J, yu Wang Z, Liu PC, jun Qu S, Huo L. Image Classification Method Based on Improved KNN Algorithm. *Journal of Physics: Conference Series*. 2021;1930(1):012009–012009. Available from: <https://dx.doi.org/10.1088/1742-6596/1930/1/012009>.
- 13) Ranadive F, Surti AZ, Patel H. Predicting Glaucoma Diagnosis Using AI. *Intelligent Systems Reference Library*. 2022;206:51–76.
- 14) Krishnan S, Amudha J, Tejwani S. Intelligent-based decision support system for diagnosing glaucoma in primary eyecare centers using eye tracker. *Journal of Intelligent & Fuzzy Systems*. 2021;41(5):5235–5242. Available from: <https://dx.doi.org/10.3233/jifs-189846>.
- 15) Li Y, Chen R, Sensale-Rodriguez B, Gao W, Yu C. Real-time multi-task diffractive deep neural networks via hardware-software co-design. *Scientific Reports*. 2021;11(1). Available from: <https://dx.doi.org/10.1038/s41598-021-90221-7>.

- 16) Chen W, Huang H, Peng S, Zhou C, Zhang C. YOLO-face: a real-time face detector. *The Visual Computer*. 2021;37:805–813. Available from: <https://dx.doi.org/10.1007/s00371-020-01831-7>.
- 17) Khosravianian A, Rahmanimanesh M, Keshavarzi P, Mozaffari S. Fast level set method for glioma brain tumor segmentation based on Superpixel fuzzy clustering and lattice Boltzmann method. *Computer Methods and Programs in Biomedicine*. 2021;198:105809–105809. Available from: <https://dx.doi.org/10.1016/j.cmpb.2020.105809>.
- 18) Ridha JA, Saud JH. Iris Segmentation Approach Based on Adaptive Threshold Value and Circular Hough Transform. *2020 International Conference on Computer Science and Software Engineering (CSASE)*. 2020;p. 32–37. doi:10.1109/CSASE48920.2020.9142123.
- 19) Jia D, Zhang C, Wu N, Guo Z, Ge H. Multi-layer segmentation framework for cell nuclei using improved GVF Snake model, Watershed, and ellipse fitting. *Biomedical Signal Processing and Control*. 2021;67:102516–102516. Available from: <https://dx.doi.org/10.1016/j.bspc.2021.102516>.
- 20) Munawar HS, '. Image and Video Processing for Defect Detection in Key Infrastructure. *Machine Vision Inspection Systems*. 2020;p. 159–177. doi:10.1002/9781119682042.ch7.
- 21) N P, D P, Mansour RF, Almazroa A. Algorithm-Based Feature Selection with Gradient Boosted Tree Model for Diabetes Classification". *Diabetes Metabolic Syndrome Obesity*. 2021;14:2789–2806. Available from: <https://doi.org/10.2147/DMSO.S312787>.
- 22) Li L, Sun L, Xue Y, Li S, Huang X, Mansour RF. Fuzzy Multilevel Image Thresholding Based on Improved Coyote Optimization Algorithm. *IEEE Access*. 2021;9:33595–33607. Available from: <https://dx.doi.org/10.1109/access.2021.3060749>.
- 23) Jha S, Seo C, Yang E, Joshi GP. Real time object detection and trackingsystem for video surveillance system. *Multimedia Tools and Applications*. 2021;80(3):3981–3996. Available from: <https://dx.doi.org/10.1007/s11042-020-09749-x>.
- 24) Malta A, Mendes M, Farinha T. Augmented Reality Maintenance Assistant Using YOLOv5. *Applied Sciences*. 2021;11(11):4758–4758. Available from: <https://dx.doi.org/10.3390/app11114758>.
- 25) Salhi A, Ghozzi F, Fakhfakh A. Estimation for Motion in Tracking and Detection Objects with Kalman Filter. *Dynamic Data Assimilation - Beating the Uncertainties*. 2020. doi:10.5772/intechopen.92863.
- 26) Bochkovskiy A, Wang CY, Liao HYM. YOLOv4: Optimal Speed and Accuracy of Object Detection. 2020. Available from: [arXiv:2004.10934v1](https://arxiv.org/abs/2004.10934v1).